PART-B

Designing of catalysts based on Nickel & Phosphomolybdic acid

CHAPTER 1

Cesium salt of nickel substituted phosphomolybdate ($PMo_{11}Ni$): Synthesis, characterization and application for hydrogenation of styrene

As mentioned in general introduction, transition metal substituted phosphomolybdate (TMSPMo$_{11}$), where M=V, Mn, Fe, Co, Ni, Cu and Zn [1-25] is most important due to the nature of transition metal, which can be tune the redox properties of PMo$_{12}$, making them important catalytic materials for the various organic transformations. Amongst this, Ni substituted phosphomolybdate is also interesting because of Lewis acidity, earth abundance and non-toxicity of Ni as well as unique redox ability of PMo$_{12}$.

In 2009, Rabia group reported oxidation of propene over ammonium salts of transition metal substituted phosphomolybdate, $(NH_4)_6HPMo_{11}MO_{40}$ (M = Ni, Co, Fe) [17]. Four years later in 2013, Patel et al. reported the one-pot synthesis of mono-transition-metal-substituted phosphomolybdates, PMo$_{11}$M (M = Co, Mn, Ni) and its catalytic efficiency was evaluated for liquid-phase solvent free alcohols oxidation [11]. Simultaneously, in the same year, same group reported Suzuki–Miyaura cross-coupling over mono-Nickel-substituted phosphomolybdates (PMo$_{11}$Ni) [23]. Further in 2014, Patel et al. [10] reported aerobic oxidation of alcohols and alkenes under solvent free condition using same catalyst as earlier reported in 2013 [11].

Also in 2017, Gangling group described the synthesis of $[PMo_{11}M(H_2O)O_{39}]^{5-}$ (M = Co^{2+}, Ni^{2+}, $Zn^{2+}$and Mn^{2+}) using the same method as reported by Patel et al. [11] and used as catalyst for catalytic oxidation desulfurization (ODS) of model oil [12]. The same group in the following year reported the synthesis of hybrids $[Bmim]_5[PMo_{11}M(H_2O)O_{39}]$ (Bmim = 1-butyl 3-methyl imidazolium; M = Co^{2+}, Ni^{2+}, Zn^{2+} and Mn^{2+}) and its catalytic activity was evaluated for the oxidation desulfurization of the model oil [13]. Mingjun et al. demonstrated solvothermal synthesis of transition metal (Fe, Co, Ni and Cu) substituted phosphomolybdate encapsulated over UiO-66 and its catalytic activity was evaluated for the aerobic epoxidation of styrene in 2021 [20]. Recently, in 2022, Wang group investigated the electrocatalytic performance of five different types transition metal substituted phosphomolybdate ($H_3PMo_{12}O_{40}$, $Na_7PMo_{11}ZnO_{40}$, $Na_7PMo_{11}CoO_{40}$, $Na_7PMo_{11}MnO_{40}$, and $Na_7PMo_{11}NiO_{40}$) for tyrosinase diphenolase activity [14].

As above literature survey shows that nickel substituted phosphomolybdate has versatile applicability in various organic transformations. However no reports are available for hydrogenation reaction. Also, p***lease note that, synthesis of cesium salt of nickel substituted phosphomolybdate (PMo$_{11}$Ni) was already reported by our group (Patel et al.) [11, 23], and well characterized by various physicochemical techniques. Its catalytic activity was evaluated for the oxidation reactions (styrene and benzyl alcohol) as well as Suzuki–Miyaura cross coupling reactions.*** As thesis consist of TMSPOMs, the said reported catalyst is also included for evaluation of its catalytic activity toward hydrogenation reactions.

In this chapter, we report the synthesis of cesium salt of nickel substituted phosphomolybdate using the same method as earlier reported by our group [11, 23]. The synthesized catalyst was characterized by basic instrumental techniques such as EDX, TGA and FT-IR. The catalytic activity of $PMo_{11}Ni$ was evaluated for styrene hydrogenation.

EXPERIMENTAL

Materials

All chemicals used were of A. R. grade. Phosphomolybdic acid, nickel acetate, cesium chloride, sodium bicarbonate, styrene, and dichloromethane obtained from Merck were used as received.

Catalyst synthesis

Cesium salt of nickel substituted phosphomolybdic acid was synthesized by using same one-pot method as described earlier by our group [11, 23]. $H_3PM_{12}O_{40}$ (1.825 g, 1 mmol) was dissolved in a minimum quantity of water and pH= 4.3 was maintained by the addition of saturated sodium bicarbonate

($NaHCO_3$). The obtained solution was heated at 80 °C with stirring and to this, a saturated solution of $Ni(CH_3CO_2)_2.4H_2O$ (0.248 gm, 1 mmol) in water, was added. The final pH of the resulting mixture was maintained at 4.3 by adding saturated $NaHCO_3$ solution, refluxed at 80 °C for 1 h and filtered hot. To this (filtrate), saturated CsCl (5 mmol, 0.8418 gm) solution was added and obtained green color precipitates were filtered, washed with water, dried at room temperature and designated as $PMo_{11}Ni$. The filtrate was used for estimation of molybdenum.

Catalytic activity

The styrene hydrogenation was carried out following the same procedure as mention in chapter 1 (Part-A).

RESULT AND DISCUSSION

Characterization

The cesium salt of nickel substituted phosphomolybdate was isolated by filtration and the remaining filtrate was analyzed for molybdenum gravimetrically [26]. The observed proportion of Mo in the filtrate was 5.4%, which corresponds to the loss of one equivalent of Mo from $H_3PMo_{12}O_{40}$.

The EDX mapping (Figure 1) confirmed the presence of Cs, P, Mo, Ni and O in the synthesized materials. The found EDX values of the elements (Cs: 25.90%, P: 1.25%, Mo: 41.34%, Ni: 2.18%, O: 28.97%) were well consistent with the that of the theoretical values (Cs:25.99%, P:1.21%, Mo: 41.28%, Ni: 2.29%, O:28.79%).

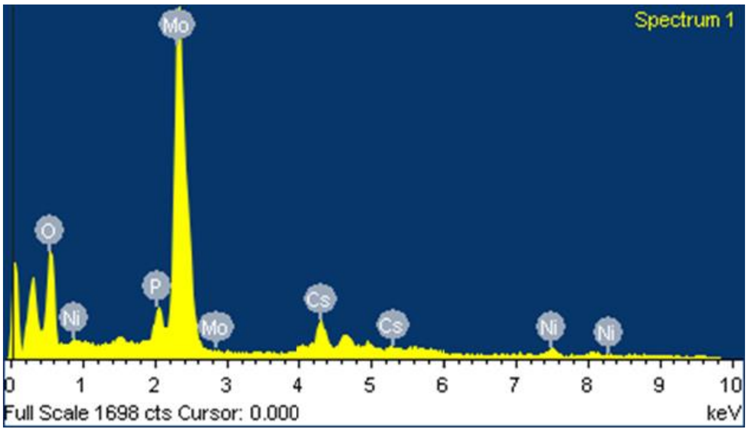

Figure 1. EDX mapping of PMo11Ni

TGA shows (Figure 2) an initial weight loss of 6.3% up to 100 °C, due to removal of adsorbed water. Further, 2.7% weight loss is observed between 150 - 300 °C which is attributed to loss of water of crystallization. No other significant weight loss indicates that the synthesized material is stable up to 500 °C. Based on the total weight loss, the number of water molecules was calculated using the formula mentioned in chapter 1 (Part A), and found to be 6. From elemental and thermal analysis, the proposed formula of the complex is $Cs_5[PMo_{11}O_{39}Ni(H_2O)].6H_2O$.

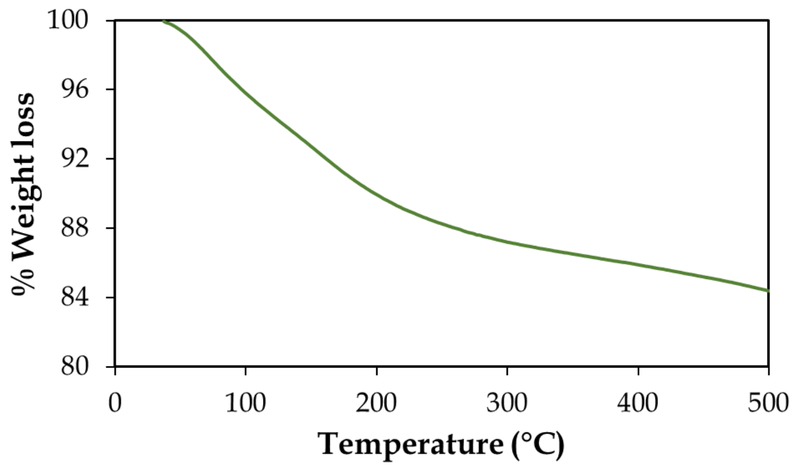

Figure 2. TGA of $PMo_{11}Ni$

The FT-IR spectra of (a) PMo_{12} (b) PMo_{11} and (c) $PMo_{11}Ni$ are shown in figure 3. The FT-IR spectra of pure PMo_{12} showed the all characteristic stretching vibration bands at 1060 cm^{-1}, 965 cm^{-1}, 870 cm^{-1} and 790 cm^{-1} which is attributed to P-O_a, Mo=O_t, Mo-O_b-Mo and v_{as} Mo-O_c-Mo stretching vibration respectively

[10, 27]. The FT-IR spectrum of PMo_{11} exhibits all the characteristic band of PMo_{12} with splitting in characteristic P-O stretching bands at 1064 and 1045 cm^{-1} which indicates the formation of a lacuna. Similarly, the spectrum of $PMo_{11}Ni$ shows all characteristics bands at 1049 cm^{-1} corresponding to P-O_a, 961 cm^{-1} corresponding to v_{as} Mo=O_t, 876 cm^{-1} corresponding to v_{as} Mo-O_b-Mo stretching and 790 cm^{-1} corresponding to v_{as} Mo-O_c-Mo stretching vibrations. Here the observed splitting in P-O band is filling by a Ni cation which restores the symmetry of the central tetrahedron, owing to the interaction between Ni and the available oxygen of the central PO_4 group (Oa). Also, it shows one additional band at 442 cm^{-1} for Ni-O stretching frequency. Obtained results are in good agreement with reported ones.

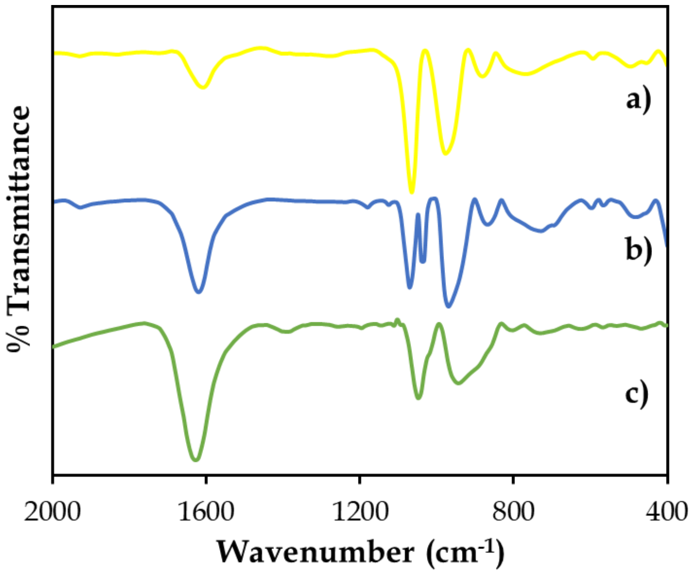

Figure 3. FT-IR spectra of (a) PMo_{12} (b) PMo_{11} and (c) $PMo_{11}Ni$

Catalytic activity

The catalytic activity of $PMo_{11}Ni$ was evaluated for styrene hydrogenation under mild reaction conditions [catalyst 5 mg, styrene (10mmol), H2 (5 bar), EtOH: H_2O (25: 25 mL), time (3h) and temperature (30 °C)]. After the completion of the reaction, obtained reaction mass was blue in colour as shown in figure 2, which indicates the catalyst degraded (decomposed) during the reaction due to the homogeneous nature. For this reason, we have not carried out its detailed catalytic studies.

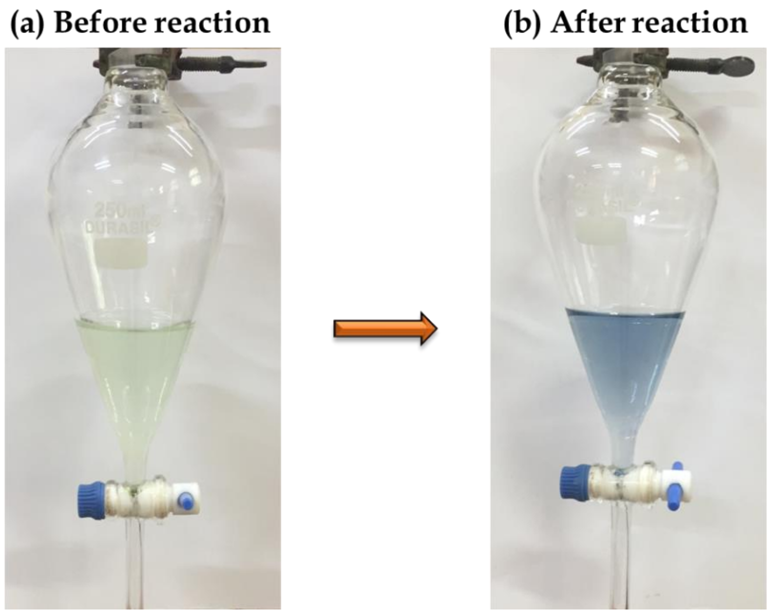

Figure 4. Color of homogeneous PMo11Ni (a)before reaction and (b) after reaction

CONCLUSION

- The designed $PMo_{11}Ni$ was found to be homogeneous in nature and therefore it reduced during hydrogenation of styrene. For this reason, we have not evaluated it for further catalytic studies.
- In short, $PMo_{11}Ni$ can be used for oxidation and Suzuki–Miyaura cross coupling but not for hydrogenation as the reaction needs par reactor with hydrogen pressure.

REFERENCES

[1] A. Patel, S. Pathan, J. Coord. Chem., 65, 3122, (2012).

[2] S. Pathan, A. Patel, Appl. Catal. A: Gen., 459, 59, (2013).

[3] S. Pathan, A. Patel, Dalton Trans., 42, 11600, (2013).

[4] S. Pathan, A. Patel, Catal. Sci. Technol., 4, 648, (2014).

[5] P. Villabrille, G. Romanelli, P. Vázquez, C. Cáceres, Appl. Catal. A: Gen., 270, 101, (2004).

[6] S. T. Yamaguchi, S. Sumimoto, Y. Ichihashi, S. Nishiyama, S. Tsuruya, Ind. Eng. Chem. Res., 44, 1, (2005).

[7] Q. Huynh, Y. Schuurman, P. Delichere, S. Loridant, J. M. M. Millet, J. Catal., 261, 166, (2009).

[8] G. Chi, Y. Qi, J. Li, L. Wang, J. Hu, J. Inorg. Biochem., 193, 173, (2019).

[9] J. Díaz, L. R. Pizzio, G. Pecchi, C. H. Campos, L. Azócar, R. Briones, R. Romero, A. Henríquez, E. M. Gaigneaux, D. Contreras, Catalysts, 12, 507, (2022).

[10] I. El Arrouji, A. Oulmekki, M. Taoufik, F. Lefebvre, J. Toyir, Mater. Today: Proc., 51, 2015, (2022).

[11] M. José da Silva, J. A. Vergara Torres, C. B. Vilanculo, RSC Adv., 12, 11796, (2022).

[12] R. Karcz, K. Pamin, J. Połtowicz, J. Haber, Catal. Lett., 132, 159, (2009).

[13] Y. Zhang, Y. Gu, X. Dong, P. Wu, Y. Li, H. Hu, G. Xue, Catal. Lett., 147, 1811, (2017).

[14] Y. Li, Y. Zhang, P. Wu, C. Feng, G. Xue, Catalysts, 8, 639, (2018).

[15] S. Cai, X. Chen, L. Wang, L. Xie, J. Liu, J. Zheng, J. Solid State Electrochem., 26, 419, (2022).

[16] C. Knapp, T. Ui, K. Nagai, N. Mizuno, Catal. Today, 71, 111, (2001).

[17] N. Mizuno, J.-S. Min, A. Taguchi, Chem. Mater., 16, 2819, (2004).

[18] T. Mazari, C. R. Marchal, S. Hocine, N. Salhi, C. Rabia, J. Nat. Gas Chem., 18, 319, (2009).

[19] R. Xing, A. Zheng, F. Wang, L. Wang, Y. Yu, A. Jiang, Food Chem., 175, 292, (2015).

[20] M. Rabbani, Z. S. Seghatoleslami, R. Rahimi, J. Mol. Struct., 1146, 113, (2017).

[21] D. Hu, X. Song, H. Zhang, X. Chang, C. Zhao, M. Jia, Mol. Catal., 506, 111552, (2021).

[22] X. Chen, J. Wang, Y. Yu, H. Chen, X. Wu, S. Gao, Catal. Lett., 152, 3807, (2022).

[23] Y. Ghandour, C. McHiri, I. Mestiri, A. Y. A. Alzahrani, H. Nasri, J. Chem. Sci., 134, 78, (2022).

[24] A. Tian, H. Ni, Y. Tian, X. Ji, G. Liu, J. Ying, Inorg. Chem. Commun., 68, 50, (2016).

[25] M. A. Rezvani, M. Shaterian, F. Akbarzadeh, S. Khandan, Chem. Eng. J., 333, 537, (2018).

[26] A. I. Vogel, J. Mendham, Vogel's Textbook of Quantitative Chemical Analysis, Pearson Education Asia, (2000).

[27] K. T. V. Rao, B. Haribabu, P. S. S. Prasad, N. Lingaiah, ChemCatChem, 4, 1173, (2012).

CHAPTER 2

Nickel exchanged phosphomolybdic acid supported on zirconia (Ni-PMo_{12}/ZrO_2): Synthesis, characterization and application for hydrogenation of Levulinic acid

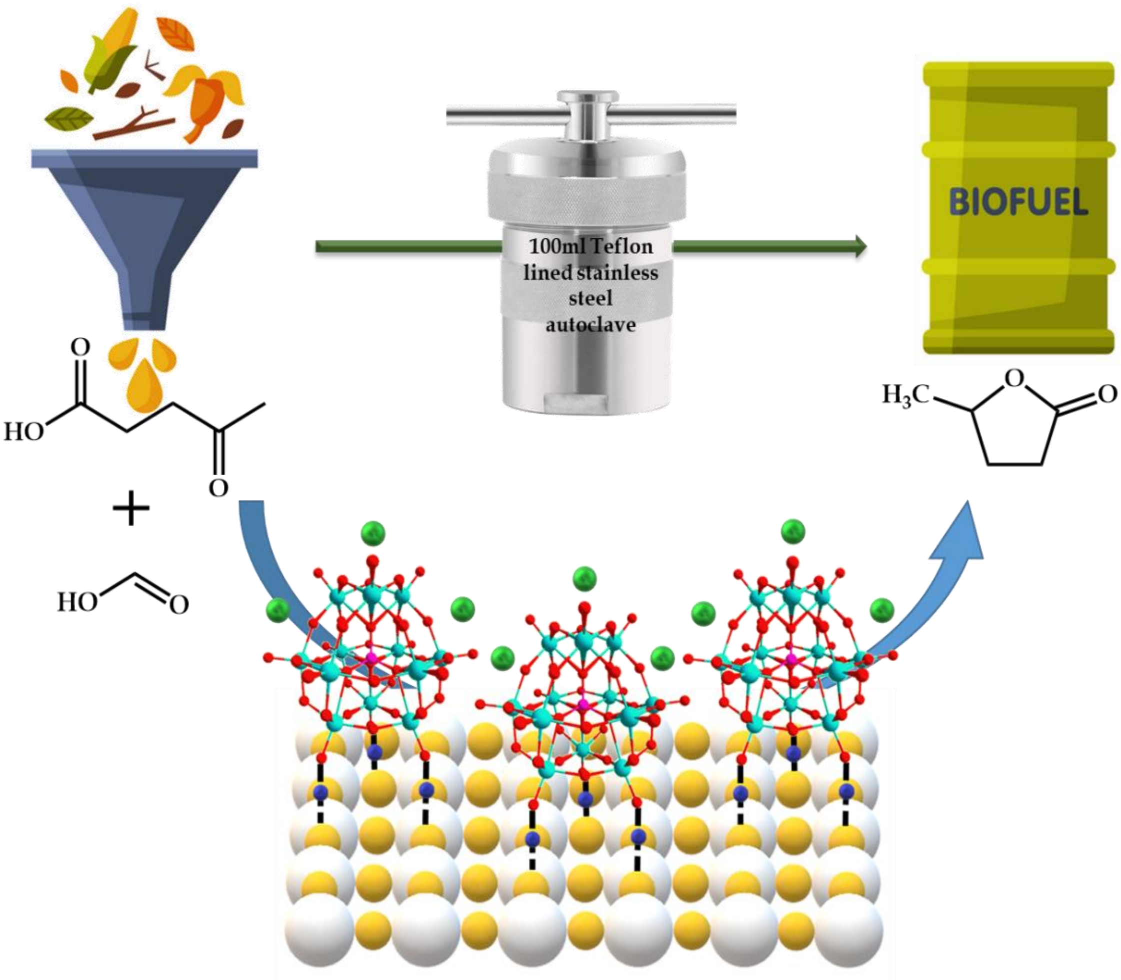

Renewable Energy 201 (2022) 190–201

Contents lists available at ScienceDirect

Renewable Energy

journal homepage: www.elsevier.com/locate/renene

Solvent free hydrogenation of levulinic acid over in-situ generated Ni(0) stabilized by supported phosphomolybdic acid using formic acid as an internal hydrogen source

Jay Patel, Anjali Patel *

Polyoxometalates and Catalysis Laboratory, Department of Chemistry, Faculty of Science, The Maharaja Sayajirao University of Baroda, Vadodara, 390002, India

A R T I C L E I N F O

Keywords:
Nickel
Phosphomolybdic acid
In-situ
Levulinic acid
Formic acid

A B S T R A C T

The present work demonstrates, in-situ generation of Ni(0) nanoparticle stabilized by phosphomolybdic acid during the reaction. Nickel exchanged supported phosphomolybdic acid, Zirconia is use as support, ($Ni–PMo_{12}/ZrO_2$) was synthesized, characterized by various physicochemical methods and its catalytic activity was evaluated for the solvent free aqueous phase hydrogenation of lignocellulosic biomass-derived levulinic acid (LA) using formic acid (FA) as internal hydrogen source. FA is promising green hydrogen storage molecule which is selectively hydrogen removed from its chemical structure and utilized it in a variety of catalytic hydrogenation reaction. FA is unique hydrogen source with high hydrogen content (4.4 wt%), low flammability, low toxicity and ease in handling as compared to other hydrogen source. To achieve outstanding performance of the catalyst, a detailed assessment of vital reaction parameters (mole ratio of FA, catalyst amount, temperature and time) were carried out. The catalyst shows outstanding activity (94% conversion) with a very low amount of Ni(0) (0.00247 mmol) and high TON (1092) for LA hydrogenation. The catalyst was found to be sustainable up to three catalytic cycles without any alteration in activity. The hot filtration test shows true heterogeneous nature of the synthesized catalyst as well as stabilizing nature of PMo_{12}. In situ formed Ni(0) was confirmed by thoroughly characterizing the regenerated catalyst by XPS, TEM, HR-TEM and STEM. The catalyst exhibits superior activity against reported catalysts. Also a plausible mechanism was proposed based on control experiments.

As described in general introduction, supported phosphomolybdic acid has gained more importance for various organic transformations due to their excellent redox properties. The PMo_{12} has available proton in secondary structure, which can be exchanged with transition metal to take the advantage of both PMo_{12} and transition metal. A literature survey on first row of transition metal shows that reports are only available on Co [1, 2], Fe [3] and Cu [4-6] exchanged supported phosphomolybdic acid.

But there is no report available on Ni exchanged supported phosphomolybdic acid. Therefore, it was thought of interest to explore Ni exchanged supported phosphomolybdic acid as Ni is an earth abundant metal and its catalytic activity was evaluated for hydrogenation of styrene and cyclohexene as mentioned in part A (Chapter 1 and 2) but we did not find any %conversion. Hence, another interesting substrate levulinic acid (LA) was selected for hydrogenation using formic acid as hydrogen source because several literature reports are available on utilization of Ni based catalysts for the same [7-14].

Recently, LA is one of the most extracted biomass-based platform molecules because of the existence of carbonyl and carboxyl groups in it [7-14]. LA is produced via hydrolysis of lignocellulosic biomass and further, it can be converted into a variety of value-added chemicals by catalytic transformations. Amongst, the hydrogenation of LA to γ-valerolactone (GVL) has gained extensive interest because GVL can be directly utilized as food additives, gasoline blenders, solvents, polymer precursors, and other valuable chemicals [7-36].

The conversion of GVL from LA, can be carried out by gaseous or liquid phase hydrogenation over homogeneous/ heterogeneous catalysts with two type of hydrogen sources, one is pressurized molecular hydrogen [7, 10-14, 18, 22-25, 30-32, 36] and other one is organic hydrogen donors [11, 12, 15-17, 19-22, 24, 26, 30, 31, 33, 34]. It is observed that catalytic transfer hydrogenation (CTH) with biomass derived hydrogen donors, i.e. Formic acid and alcohols are found to be more sustainable in terms of availability, use and handling [15-17, 19-21, 26, 33, 34]. Formic acid (FA) has gained tremendous attention, as it is obtained as an equivalent by-product during LA production in biorefineries [33]. Also, FA is safer in terms of low operational risk, easy storage and transportation as compared to high-pressure H_2 gas.

As mentioned earlier, amongst the available reports on Ni based catalyst for LA hydrogenation, many groups have reported the synthesis of Ni based bimetallic catalyst, where it requires high amount of Ni as well as complex synthetic procedure including high temperature pyrolysis and calcination. Furthermore, the synthesized supported Ni nanoparticles suffer from deactivation during harsh reaction conditions leading to leaching or sintering [20, 21, 26-29, 34, 35]. Hence, it is necessary to design a stabilized NiNPs with highly dispersion. Towards the same, Srinivasan et. al. reported in-situ generated Ni(0)@boehmite, as an efficient catalyst for the selective preparation of GVL from LA, in which first they synthesized NiAl-LDH by co-precipitation method and during the reaction Ni(II) reduce in to Ni(0) state [18].

Thus, it seems that the designing of stabilized Ni(0) based catalysts are of great importance and a challenge also. Keeping in mind the present scenario, we have thought to design a catalyst comprising of Ni and phosphomolybdic acid as they have fascinating diverse convergent properties. These properties include the robust oxoanionic nature, negative charges, large relative sizes, reducing and encapsulating agents, and as a result, they perform as excellent stabilizing agents to stabilize Ni nano particles with high surface free energy and high dispersion [37, 38] by preventing agglomeration.

In present chapter, we first time report highly sustainable and stabilized in-situ formation of nickel nanoparticles (NiNPs), during the reaction from Ni (II) exchanged phosphomolybdic acid (PMo_{12}) supported on to hydrous zirconia (ZrO_2). The synthesized catalyst was characterized thoroughly by various physicochemical techniques. The catalytic efficiency of synthesized catalyst was evaluated for solvent free hydrogenation of LA using formic acid (FA) as an internal H-donor. The effect of catalyst amount, solvent, FA, temperature, and time were studied to achieve maximum % conversion and selectivity. The hot filtration test was carried out to evaluate the heterogeneity of catalyst. The catalyst was recycled by simple centrifugation and reused up to three cycles under optimized conditions. The regenerated catalyst was characterized by FT-IR, XPS, HRTEM and HAADF-STEM to confirm the in-situ formation of Ni NPs and stability of the catalyst. The catalytic activity of the present catalyst was compared with reported one. The catalyst exhibits superior activity against reported catalysts. Further, a probable reaction mechanism was proposed based on control experiments study.

EXPERIMENTAL

Materials

All chemicals used were of A.R. grade. Phosphomolybdic acid ($PMo_{12}O_{40}$), nickel acetate [$Ni(CH_3CO_2)_2.4H_2O$], zirconium oxychloride ($ZrOCl_2 \cdot 8H_2O$), ammonia (25% w/v), levulinic acid and dichloromethane (DCM) were used as received from Merck. Formic acid was acquired from Avra Synthesis Pvt. Ltd.

Catalyst synthesis

Nickel exchanged phosphomolybdic acid supported on zirconia was synthesized by following three steps.

Step-1: Synthesis of Zirconia (ZrO_2)

ZrO_2 was synthesized as described in Chapter 2 (Part A) [39].

Step-2: Synthesis of phosphomolybdic acid supported on zirconia (PMo_{12}/ZrO_2):

PMo_{12}/ZrO_2 was synthesized as described in Chapter 2 (Part A) [39].

Step-3: Synthesis of Nickel exchanged phosphomolybdic acid supported on zirconia (Ni-PMo_{12}/ZrO_2):

Nickel (Ni) was deposited by exchanging available counter protons of PMo_{12} in PMo_{12}/ZrO_2. 1 g of PMo_{12}/ZrO_2 was soaked in 25 mL 0.04 M $Ni(CH_3CO_2)_2.4H_2O$ aqueous solution with intermittent stirring for 24 hours. The mixture was filtered, then washed with distilled water to remove excess of Ni and air dried at room temperature. The obtained green color material was designated as Ni-PMo_{12}/ZrO_2 (Scheme 1).

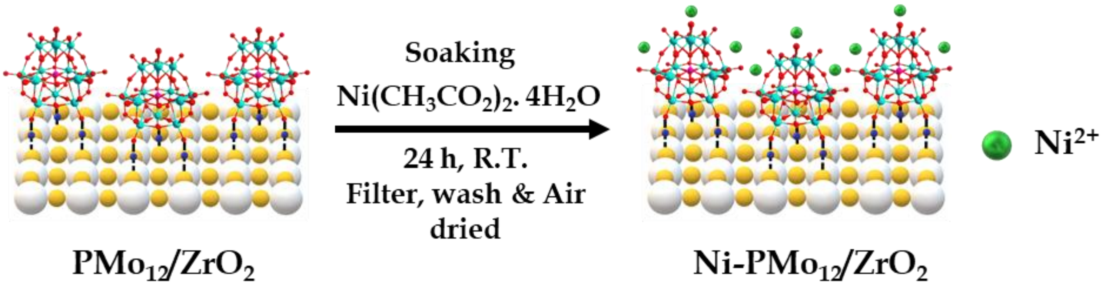

Scheme 1. Synthesis of Ni-PMo_{12}/ZrO_2

Catalytic activity

The hydrogenation of levulinic acid (LA) to γ- valerolactone (GVL) was carried out in Teflon lined stainless-steel autoclave (made in-house) having 25 mL volume capacity. In a typical experiment, LA, FA (hydrogen source) and catalyst was charge into the Teflon container. Finally, the autoclave was sealed and put in to oven at 200 °C for 6 h. After completion of the reaction, the autoclave was cooled down, the remaining pressure was released and the organic layer was extracted using dichloromethane, whereas catalyst was collected from the junction of the liquid phase and finally recovered by centrifugation. The organic phase was dried with anhydrous magnesium sulfate and analyzed by a gas chromatograph (Shimadzu-2014) using a capillary column (RTX-5). The product was identified by comparing with standard samples. The schematic representation of catalytic methodology is represented in Scheme 2.

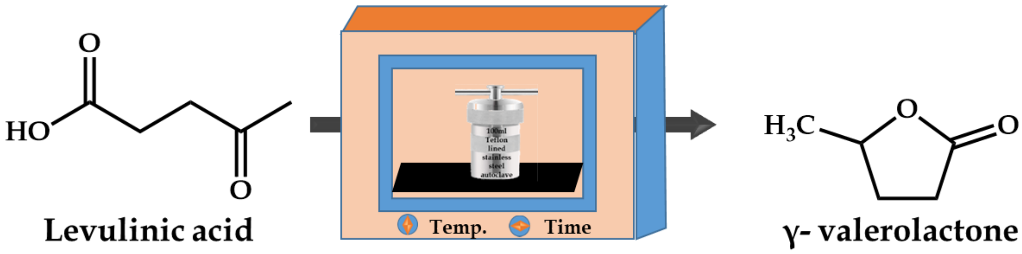

Scheme 2. Schematic presentation of LA hydrogenation

RESULT AND DISCUSSION

Characterization

The amount of Ni in synthesized Ni-PMo_{12}/ZrO_2 was determined by volumetric analysis of Ni in standard nickel acetate solution and in the filtrate [39]. The amount of Ni was found to be 0.27 wt%. EDX mapping (Figure 1) shows the presence of all the elements (P, Ni, Mo, O and Zr). The found EDX values of Ni and Mo (0.29 wt% and 14.31 wt% respectively) are in good agreement with theoretical values (0.30 wt% and 14.29 wt% respectively). Here, very low 0.29 wt% of Ni, indicates that it is exchanged only with the available protons of PMo_{12}/ZrO_2.

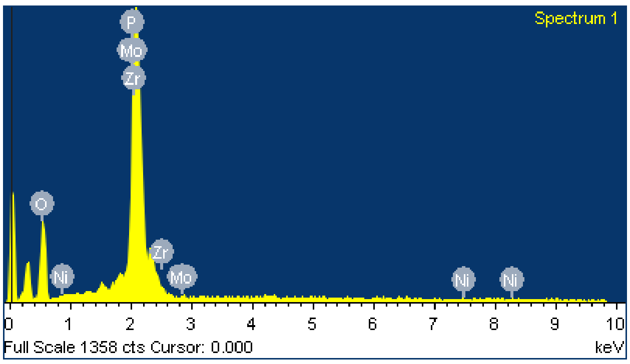

Figure 1. EDX mapping of Ni-PMo_{12}/ZrO_2

The thermal stability of PMo_{12}/ZrO_2 and Ni- PMo_{12}/ZrO_2 was determined using TGA (Figure 2). TGA curve of PMo_{12}/ZrO_2 shows 5.3% weight loss up to 100 °C, which is attributed to the loss of adsorbed water. Further, it shows 6.4% weight loss up to 300 °C corresponds to the loss of crystalline water molecules present in PMo_{12}. After that, no further weight loss up to 500 °C indicates the stability of

PMo_{12}/ZrO_2. The TGA of Ni-PMo_{12}/ZrO_2 shows initial 8.7% weight loss up to 150 °C, which is attributed to removal of physically adsorbed water molecules. The second weight loss, which occurs between 150 to 250 °C is due to the removal of water of crystallization which resulted in the formation of the Kaggin structure. Beside this, no significant weight loss is observed up to 500 °C which attributes to high thermal stability of Ni-PMo_{12}/ZrO_2. Similarly, the TGA of Ni/ZrO_2 shows 9.8% weight loss up to 150 °C because of the removal of adsorbed water.

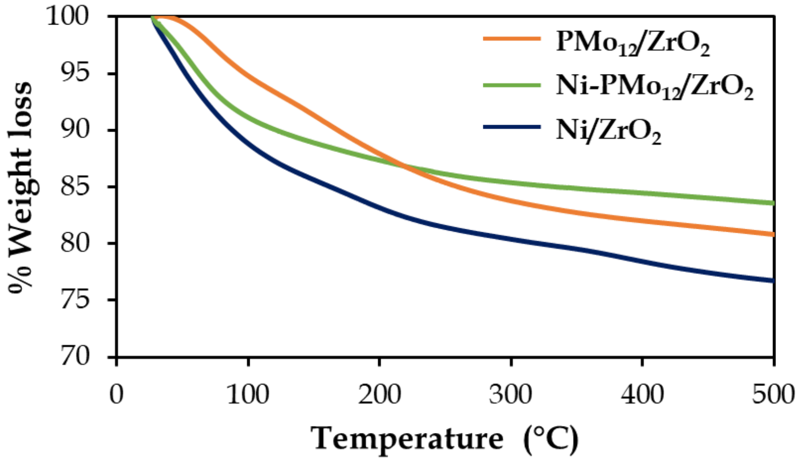

Figure 2. TGA curve of PMo_{12}/ZrO_2, Ni-PMo_{12}/ZrO_2 and Ni/ZrO_2

The FT-IR spectra of ZrO_2, Ni/ZrO_2, PMo_{12}, PMo_{12}/ZrO_2 and Ni- PMo_{12}/ZrO_2 are displayed in figure 3. FT-IR spectrum of ZrO_2 (Figure 3a) shows bands at 1600 cm^{-1}, 1370 cm^{-1} and 600 cm^{-1}, corresponding to asymmetric H–O–H stretching, O–H–O and Zr-O-H bending vibrations respectively [38, 39]. Similarly, the FT-IR spectra of Ni/ZrO_2 shows (Figure 3b) all bands of ZrO_2 and the additional band attributed to Ni-O was not appeared because of superimposition of Zr-O-H broad band. [38]. The FT-IR spectra of PMo_{12} (Figure 3c) show typical band of Keggin unit at 1060 cm^{-1} attributed to central P-O stretching, at 965 cm^{-1} attributed to terminal Mo=O stretching and bands at 870 and 790 cm^{-1} corner shared and edge shared Mo-O-Mo stretching. [39] Similarly, PMo_{12}/ZrO_2 (Figure 3d) shows all the three characteristic finger print band of PMo_{12} without any significant change at 1065, 965, 872 cm^{-1} corresponding to P-O, Mo=O and Mo-O-Mo stretching vibration frequency respectively as well as band at 1605, 1379 and 600 cm^{-1} attributed to H–O–H, O–H–O and Zr-O-H stretching frequency respectively, indicating that the retention of Keggin unit (PMo_{12}) after support on ZrO_2 [39]. The FT-IR spectra spectrum of Ni-PMo_{12}/ZrO_2 (Figure 3e) also shows all the characteristic band of PMo_{12}/ZrO_2 with slight shifting at 1065 cm^{-1} (P-O), 965 cm^{-1} (Mo=O), 881 cm^{-1} (Mo-O-Mo), 1605 cm^{-1} (H–O–H), 1379 cm^{-1} (O–H–O) and 600 cm^{-1} (Zr-O-H). This obtained shifting is due to the Ni exchanged with available proton of PMo_{12}. However, the additional band attributed to Ni-O was not observed due to the superimposition with the band of ZrO_2. It is interesting to note down that, if Ni would have been in to the lacuna, the P-O band would have split. However, there was no splitting, indicating that Ni is not inserted into lacuna, and as a counter cation only.

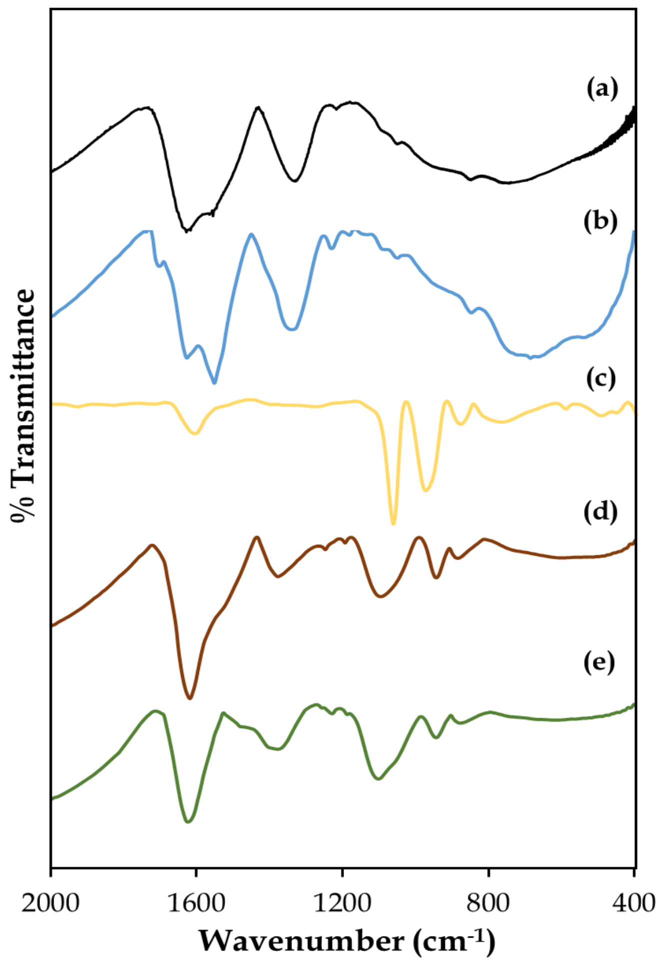

Figure 3. FT-IR Spectra of (a) ZrO_2, (b) Ni/ZrO_2, (c) PMo_{12}, (d) PMo_{12}/ZrO_2 and (e) Ni-PMo_{12}/ZrO_2

To understand the chemical environment around central phosphorus atom in PMo_{12} as well as the interaction between the Keggin anion with support, ^{31}P MAS NMR of PMo_{12}, PMo_{12}/ZrO_2 and Ni-PMo_{12}/ZrO_2 were carried out (Figure 4). ^{31}P NMR of Pure PMo_{12} (Figure 4a) shows a single at -3.815 ppm, which is good agreement with the reported one [40]. Whereas PMo_{12}/ZrO_2 (Figure 4b) exhibits intense peak with slight up filed shifting from -3.815 to -4.109 ppm as compared to pure PMo_{12}, because of the terminal oxygen (Mo=O_t) of PMo_{12} interact with hydrogen of ZrO_2 (Zr-O-H) to form O_t-H-O (Mo=O_t-H-O-ZrO_2) bond during synthesis [37, 40]. In the case of Ni-$PMo_{12}/ZrO_{2,}$ ^{31}P NMR (Figure 4c) shows intense peak at -7.580 ppm with significant up filed shifting due to Ni exchanged with available counter cation proton of PMo_{12}.

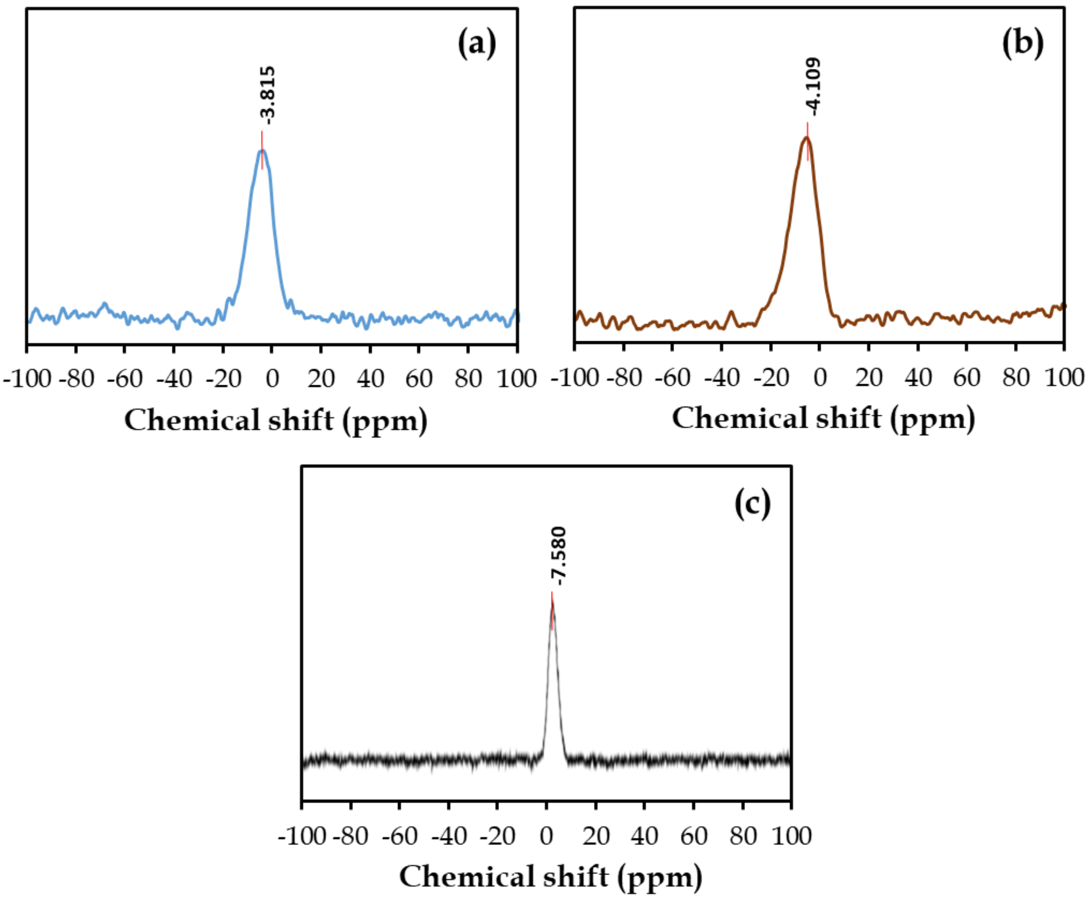

Figure 4. ^{31}P MAS NMR of (a) PMo_{12}, (b) PMo_{12}/ZrO_2 and (c) Ni- PMo_{12}/ZrO_2

The high resolution XPS of Ni-PMo_{12}/ZrO_2 was carried to confirm the electronic state of all present elements (Zr, Ni, Mo and O). In figure 5, obtained spectra shows low intense peak at binding energy 854.5 eV corresponding to Ni $2p_{3/2}$ spin orbit confirming the presence of Ni(II) [11, 16, 18, 22-25, 30-33, 36]. Also it shows two well resolved spin–orbit doublet correspond to Mo, (i) at binding energy 233 and 235 eV corresponding to $3d_{5/2}$ and $3d_{3/2}$ energy levels (ii) at binding energy 397, and 416 eV respectively for $3p_{3/2}$ and $3p_{1/2}$ energy level which confirms presence of Mo(VI) in the synthesized material [37, 40]. A very intense peak at binding energy 591 attributes to O1s spin-orbit of oxygen, present in PMo_{12} and ZrO_2. Two additional high intense peaks at binding energy 331 and 345 eV attributes to $Zr3p_{3/2}$ and $Zr3p_{1/2}$, respectively [38-40]. However, obtained very low intense peak correspond to Ni because of very low amount of Ni (0.29 wt%) in Ni-PMo_{12}/ZrO_2.

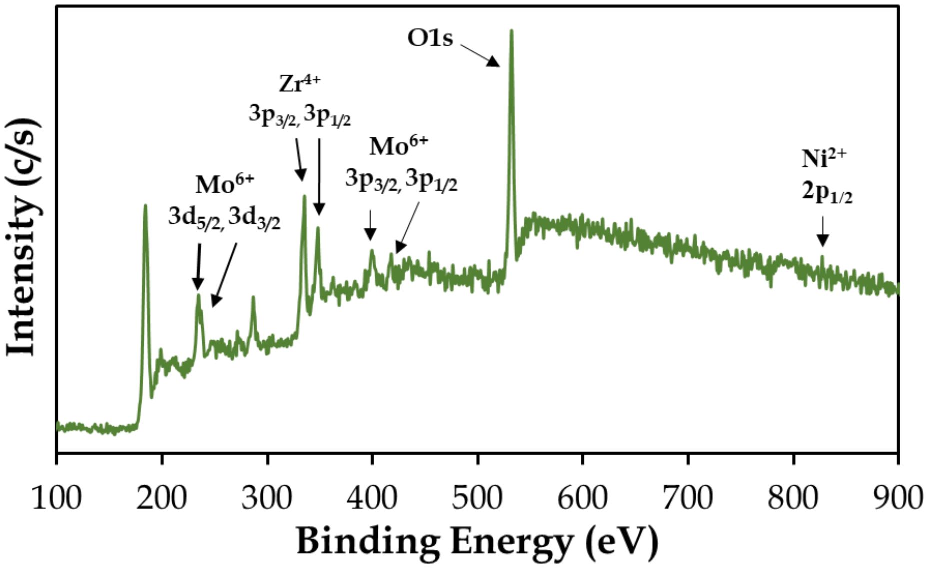

Figure 5. XPS spectra of Ni-PMo_{12}/ZrO_2

The N_2 adsorption desorption isotherms of ZrO_2, PMo_{12}/ZrO_2 and Ni-PMo_{12}/ZrO_2 are shown in figure 6. The nature of N_2 adsorption desorption isotherms of PMo_{12}/ZrO_2 and Ni-PMo_{12}/ZrO_2 are similar to that of ZrO_2 even after supporting PMo_{12} on ZrO_2 as well as after exchanging Ni with available protons in PMo_{12}/ZrO_2. This shows the retention of basic structure with high dispersion. The BET surface area of ZrO_2 was found to be 170 m^2g^{-1} [38]. As expected, the significant higher surface area was obtained in case of PMo_{12}/ZrO_2 (204 m^2 g^{-1}) which is due to high desperation of PMo_{12} on ZrO_2 [41]. However, a slight increase in surface area from 204 to 207 m^2g^{-1} for Ni-PMo_{12}/ZrO_2 may be due to the presence of Ni as counteraction (as a result of exchange with available protons of PMo_{12}) only.

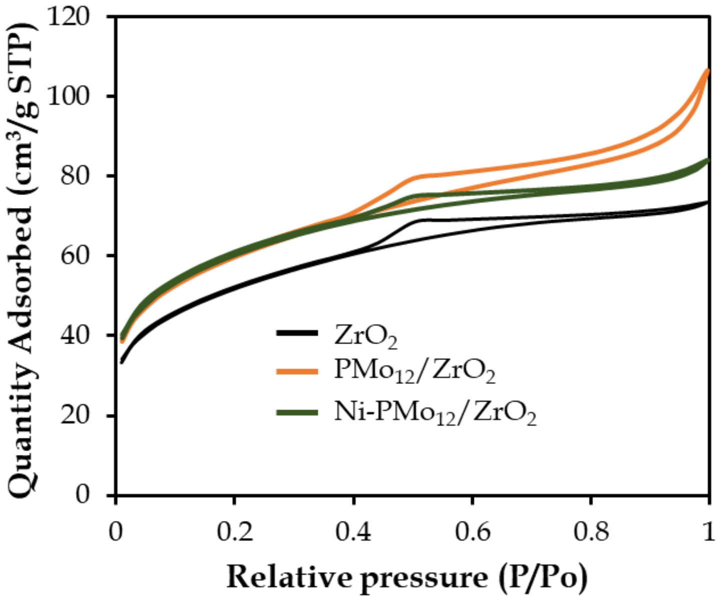

Figure 6. N_2 adsorption desorption isotherm of ZrO_2, PMo_{12}/ZrO_2 and Ni-PMo_{12}/ZrO_2

The XRD patterns of PMo_{12}, ZrO_2, PMo_{12}/ZrO_2 and Ni-PMo_{12}/ZrO_2 were recorded (Figure 7). The XRD pattern of PMo_{12} show (Figure 7a) all characteristic peaks at 2θ in the range of 20 to 35 degree [40]. The characteristic broad peaks (Figure 7b) between 25°- 35° indicate the amorphous nature of the ZrO_2 support [38-40]. The XRD patterns PMo_{12}/ZrO_2 (Figure 7c) shows absence of all characteristic peaks of PMo_{12} which indicates the uniform dispersion of PMo_{12} on the surface of ZrO_2 support [40]. Similarly, Ni-PMo_{12}/ZrO_2 (Figure 7d) did not show any characteristic diffraction peaks Ni as well as PMo_{12}, indicates that high desperation on support ZrO_2 surface during the synthesis.

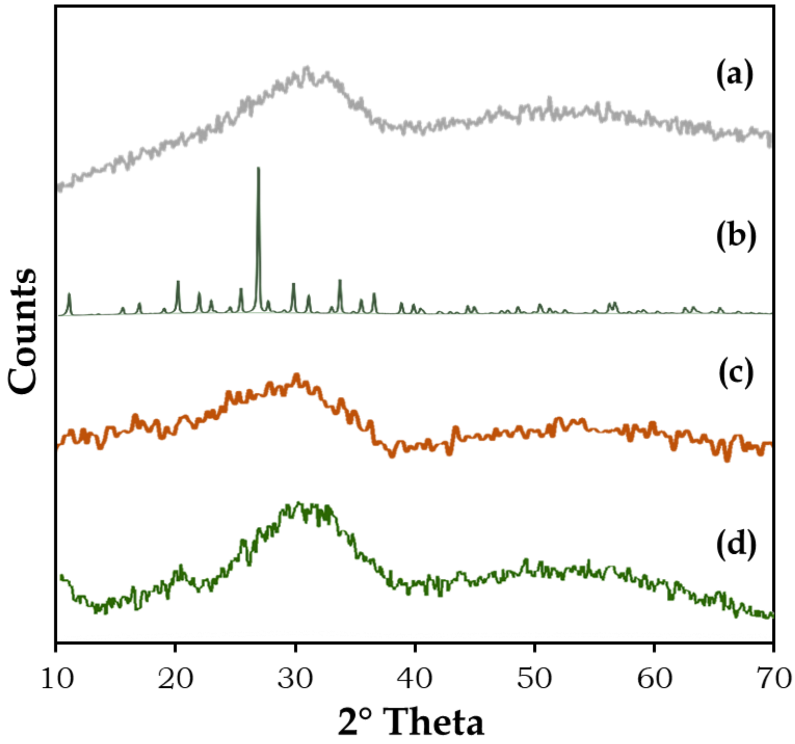

Figure 7. Powder XRD pattern of (a) ZrO_2, (b) PMo_{12}, (c) PMo_{12}/ZrO_2 and (d) Ni- PMo_{12}/ZrO_2

Catalytic activity

As mentioned in introduction, the synthesized catalyst (Ni-PMo_{12}/ZrO_2) was inactive towards styrene and cyclohexene hydrogenation under optimized conditions; (i) catalyst (5 mg) styrene (10 mmol), EtOH: H_2O (30:20 mL), H_2 pressure (5 bar), time (3 h), temperature (30 °C) and (ii) catalyst amount (25 mg), cyclohexene (9.87 mmol), H_2O (50 mL), H_2 pressure (10 bar), time (2 h) and temperature (50 °C) as described in part A (Chapter 1 and 2) respectively. Also, it is worth to note down that for Ni catalyzed hydrogenation reaction, Ni must be present in Ni(0) state. However, conversion of Ni(2+) to Ni(0) requires harsh conditions, as mentioned in reported articles. Under harsh conditions, PMo_{12} my gets decomposed and therefore, we have thought to utilize formic acid, as an internal hydrogen source because it is most sustainable amongst the available ones.

Further, the catalytic efficiency of synthesized catalyst, Ni-PMo_{12}/ZrO_2 was evaluated for liquid phase LA hydrogenation reaction using FA as internal hydrogen source. To achieve maximum conversion various reaction parameters such as amount of catalyst, effect of FA, time and temperature were optimized.

The effect of catalyst to LA ratio was optimized by catalyst amount varying from 30 mg to 60 mg with 10 mg interval and obtained results are depicted in figure 8a. From the figure 8a it can be seen that % conversion of LA to GVL increased with rise in amount of catalyst i.e. amount Ni mol% up to 50 mg. Because an increase in catalyst amount increases the Ni active site which accelerates the rate of reaction via thermal decomposition of FA. However, with further increasing in catalyst amount (60 mg) there was no significant change found in %conversion (2%). Based on the obtained results, 50 mg of catalyst was optimized for the further optimization studies.

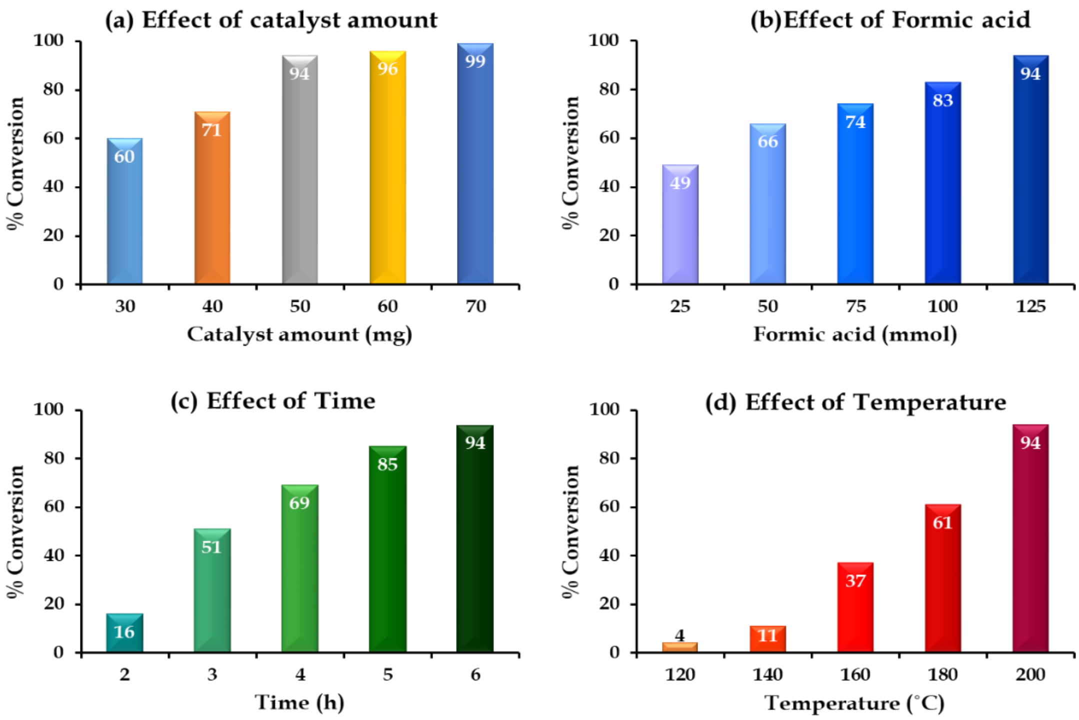

Figure 8. Optimization of reaction parameters for LA hydrogenation. Reaction conditions: (a) Effect of catalyst amount- LA (5 mmol), FA (125 mmol), time (6 h) and temperature (200 °C); (b) Effect of Formic acid- LA (5 mmol), catalyst (50 mg), time (6 h) and temperature (200 °C); (c) Effect of time. LA (5 mmol), FA (125 mmol), catalyst (50 mg) and temperature (200 °C); (d) Effect of temperature- LA (5 mmol), FA (125 mmol), catalyst (50 mg) and time (6 h).

The effect of FA as internal hydrogen donor was studied by change in mole ratio of LA to FA from 1:5 to 1:125 mmol. The obtained result (Figure 8b) suggested that with increasing mole ratio of FA from 5 to 125 mmol within interval of 25 mmol, also increased in the % conversion (from 49 to 94% respectively) of LA. Here, a large amount of FA was required as we expected in-situ reduction of Ni(II) to Ni(0), which is confirmed by characterization of regenerated catalyst.

The effect of reaction time was also screened in order to achieve maximum conversion and the obtained results are presented in figure 8c. From the figure 8, it is seen that with increase in time from 2 h to 6 h, % conversion increases gradually from 16% to 94% respectively. The obtained results are in good agreement with the well-known fact that with increase in time, there is increase in formation of reactive intermediates from reactants which is further converted into products. Based on this, 6 h was optimized to achieve 94% conversion.

Influence of temperature was assessed between 120 and 200 °C with interval of 20 °C. The obtained result (Figure 8d) shows the %conversion increased with increase in temperature which may be due to the fact that at higher temperature FA easily decomposed to form internal hydrogen to further transform of LA to GVL. Therefore, based on this 200 °C temperature was optimized to achieve maximum 94% conversion.

Based on this study, the optimized conditions for 94% conversion are: Catalyst amount (50 mg), active amount of Ni ($2.47 * 10^{-3}$ mmol), LA (5 mmol), substrate /catalyst ratio (2024), FA (125 mmol), time (6 h) and temperature (200 °C) with TON (1902).

The gas chromatograph of optimized reaction conditions for LA hydrogenation is shown in figure 9.

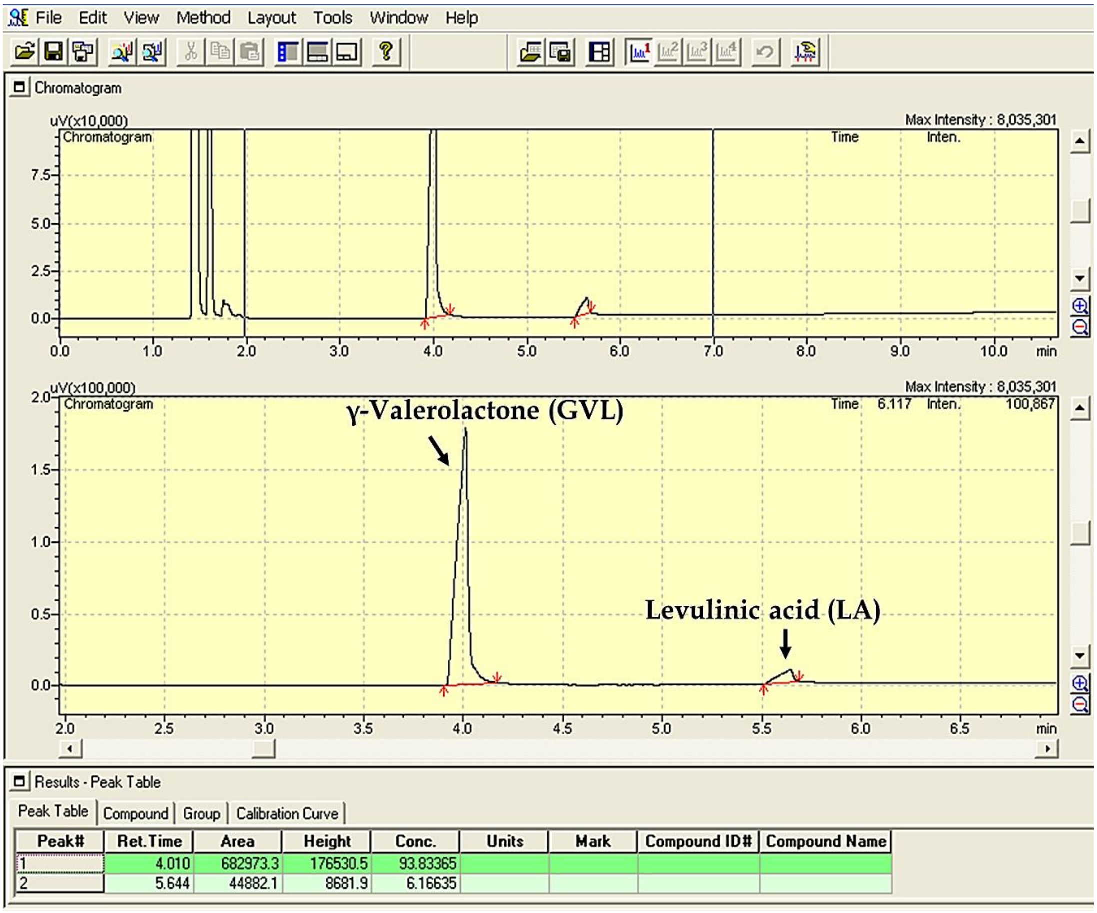

Figure 9. Gas chromatograph of LA hydrogenation

Control experiment

The control experiments were carried out under optimized conditions with PMo_{12}, ZrO_2, PMo_{12}/ZrO_2, $Ni(CH_3CO_2)_2$ and Ni/ZrO_2 to understand the role of each component in synthesized catalyst Ni-PMo_{12}/ZrO_2. The obtained results are displayed in the table 1. From the table it can be seen that PMo_{12}, ZrO_2, PMo_{12}/ZrO_2 is totally inactive towards the reaction. However, $Ni(CH_3CO_2)_2$, Ni/ZrO_2 and Ni-PMo_{12}/ZrO_2 are given almost same conversion (88%, 91% and 94% respectively). Based on this study the obtained result confirmed that Ni is the only active species for the reaction progress.

Table 1. Control experiment

Catalyst	%Conversion	% Selectivity
[a]ZrO_2	NA	NA
[b]PMo_{12}	NA	NA
[c]PMo_{12}/ZrO_2	NA	NA
[d] $Ni(CH_3CO_2)_2$	88	100
[e]Ni/ZrO_2	91	100
$Ni\text{-}PMo_{12}/ZrO_2$	94	100

Reaction conditions: Catalyst ([a]38.45 mg, [b]11.5 mg, [c]47.75 mg, [d]5 mg, [e]38.45mg, 50 mg, [d,e]Ni: $2.47*10^{-3}$ mmol), LA (5 mmol), FA (125 mmol), time (6 h) and temperature (200 °C).

Hot filtration and heterogeneity test

One of the most basic requirements in heterogeneous catalysis is that the catalyst should retain its heterogeneity while keeping its active sites intact over several cycles. Hot filtration test was carried out in order to investigate leaching of Ni from $Ni\text{-}PMo_{12}/ZrO_2$ as well as Ni/ZrO_2 in the optimized reaction condition. Initially the reaction was carried out with $Ni\text{-}PMo_{12}/ZrO_2$ and Ni/ZrO_2 up to 3 h, after that the catalyst was removed by the centrifugation, and then further reaction was carried out with resultant filtrate up to 6h (another 3h). After the reaction was completed, the organic layer was extracted with dichloromethane and analyzed using a gas chromatogram. In case of Ni/ZrO_2 obtained result shows significant increase in %conversion of LA after removing catalyst. The obtained result (Table 2) indicates the leaching of Ni from the supports (ZrO_2) during the reaction. However, in case of $Ni\text{-}PMo_{12}/ZrO_2$, after removing the catalyst, the obtained result shows that there is no significant change in % conversion, indicating that Ni is not leached during the reaction. Also, confirmed that PMo_{12} act as stabilizing agent for Ni during the reaction. These obtained results further confirm that synthesized catalyst ($Ni\text{-}PMo_{12}/ZrO_2$) is truly heterogeneous which is also reflected in recycling study.

Table 2. Hot filtration test

Catalyst	%Conversion	% Selectivity
[a]Ni/ZrO_2	50 (after 3 h) 61 (after 6 h)	100
[b]$Ni\text{-}PMo_{12}/ZrO_2$	52 (after 3 h) 53 (after 6 h)	100

Reaction conditions: Catalyst ([a]38.45 mg, [b]50 mg, [a,b]Ni: $2.47*10^{-3}$ mmol), LA (5 mmol), FA (125 mmol), time (6 h) and temperature (200 °C).

Regeneration and recycling studies

The catalyst sustainability is key issue for any catalytic process. Taking into consideration, after completion of reaction the catalyst was centrifuged and washed with dichloromethane, water, and finally air-dried after reaction completion for reuse in the next catalytic cycle. From the table 3 it is seen that, there is no appreciable change in % conversion up to three catalytic runs. This study clearly shows that catalyst was sustainable and truly heterogeneous in nature which is simply regenerated and reused up to three cycles and also can be reused for further cycles which depends on choice of the chemist. This clearly shows that the synthesized catalyst is truly heterogeneous in nature.

Table 3. Catalyst reusability

Catalyst	% Conversion
Fresh	94
R-1	94
R-2	93
R-3	93

Reaction conditions: Catalyst (50 mg), LA (5 mmol), FA (125 mmol), time (6 h) and temperature (200 °C).

Characterization of regenerated catalyst and conformation of Ni(0)

After the reaction was carried out under optimized condition, the obtained used catalyst (regenerated catalyst) was found to be in black color instead light green color as shown in the figure 10. It is the first indication that Ni(II) gets reduced to N(0). This is further confirmed by systemic characterization of the regenerated Ni-PMo_{12}/ZrO_2, using various physicochemical techniques, i.e., BET, EDX, FT-IR, XPS, XRD, TEM, HR-TEM and STEM.

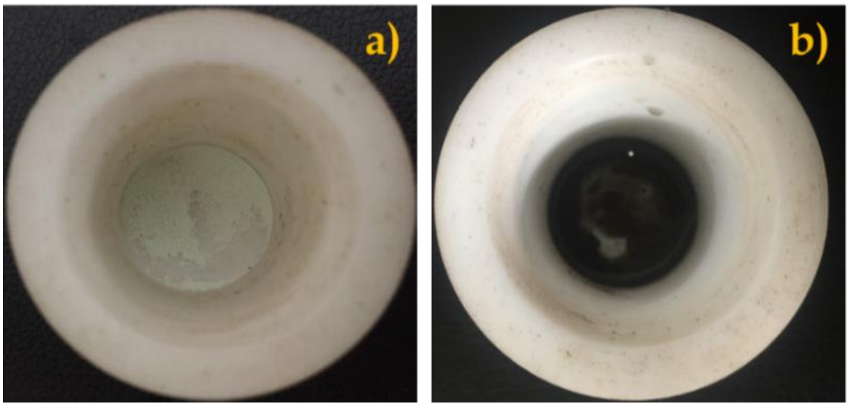

Figure 10. a) catalyst color before reaction and b) catalyst color after reaction

First BET surface area of the regenerated Ni-PMo_{12}/ZrO_2 was carried out and it was found that there is a drastic increase in BET surface area of the regenerated catalyst (219 m^2/g) as compared to fresh catalyst (207 m^2/g), which indicates the formation of Ni(0) nanoparticles during the reaction. Also, the nitrogen adsorption desorption isotherm of regenerated catalyst Ni-PMo_{12}/ZrO_2 is almost identical (Figure 11) as compared to that of fresh catalyst (Ni-PMo_{12}/ZrO_2) which indicates that surface phenomena remain intact even after regeneration.

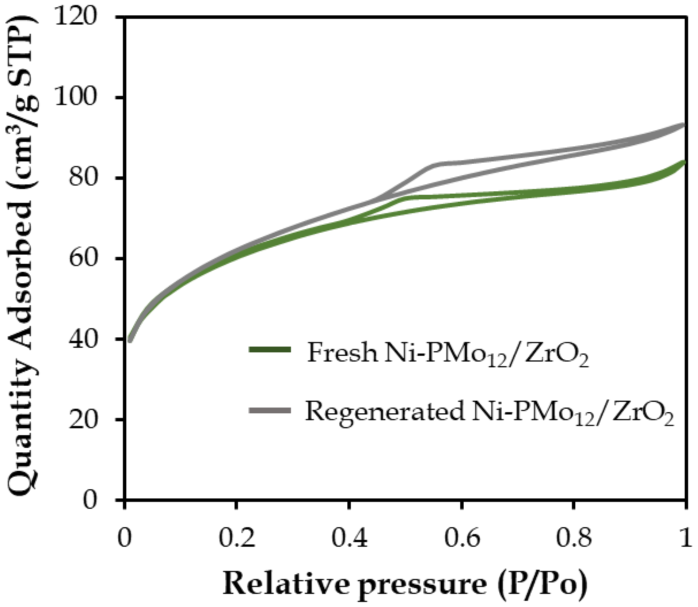

Figure 11. BET adsorption desorption isotherm of fresh and regenerated Ni-PMo_{12}/ZrO_2

The XPS analysis of the regenerated Ni-PMo_{12}/ZrO_2 (Figure 12) reveals that all the characteristic binding energy peak of Mo, Zr, and O are identical to those found in the fresh catalyst (Figure 5). However, low intense binding energy peak corresponds to Ni shifting from 854.5 eV to 852.1 eV [42], indicating the formation of Ni nanoparticles during the reaction. Two well resolved spin–orbit doublet corresponds to Mo(VI) which confirms that PMo_{12} stabilizes the Ni NPs formed in situ during the reaction.

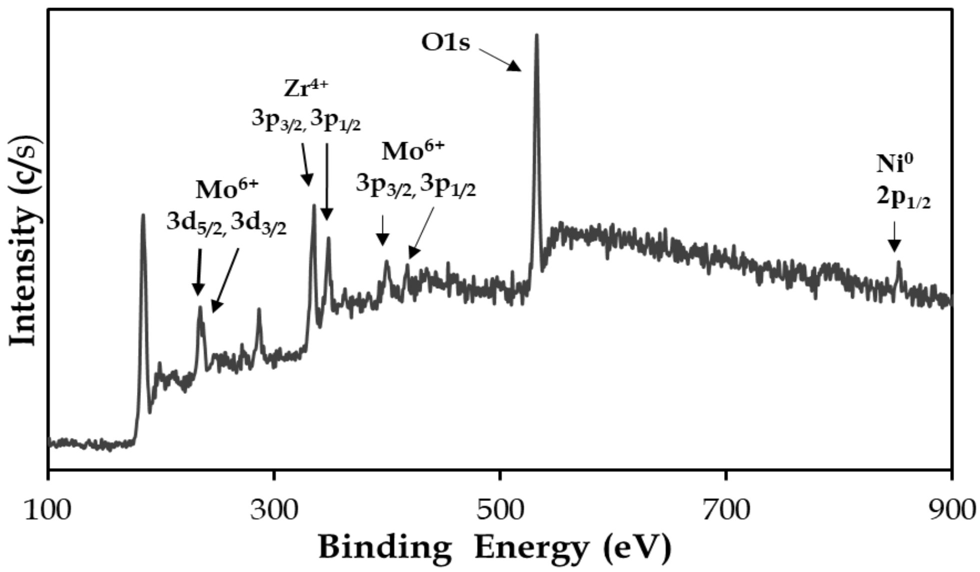

Figure 12. XPS spectra of regenerated Ni-PMo_{12}/ZrO_2

TEM micrograph of regenerated Ni–PMo_{12}/ZrO_2 with different magnifications are shown in figure 13a-c. Images does not show NiNPs because of high dispersion on amorphous nature of the catalyst which suggests that the size of Ni particles is beyond the detection limit of TEM. To further confirm this, HRTEM micrographs were also recorded as shown in figure 13d-e. It clearly shows that the size of Ni particle is <5 nm as well as there is a uniform dispersion of Ni throughout the morphology, without the formation of any aggregates, thereby confirming the stabilization of NiNPs by PMo_{12}.

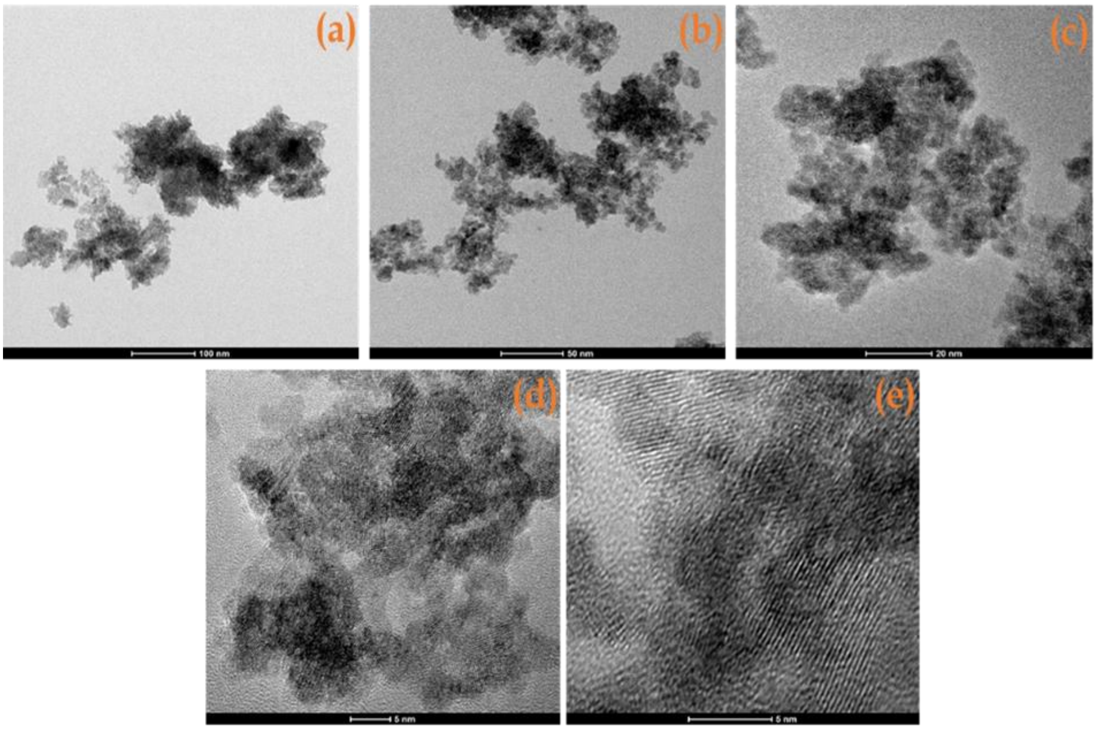

Figure 13. (a-c) TEM images and (d-e) HR-TEM images of regenerated Ni-PMo_{12}/ZrO_2

For more insight of NiNPs, an advanced analysis, i.e., HAADF-STEM with coupled EDX analysis measurements was performed (Figure 14a-g). HAADF-STEM images (Figure 14a-g) show homogeneous dispersion of Ni on the PMo_{12}/ZrO_2 surface. Whereas, the STEM EDX mapping image of Ni (Figure 14e) and the overlapping image (Figure 14g) clearly shows the presence of isolated NiNPs with a homogeneous dispersion with no cross-linkage. EDX (Figure 14b-g) also confirm the presence of all possible elements in the synthesized catalyst.

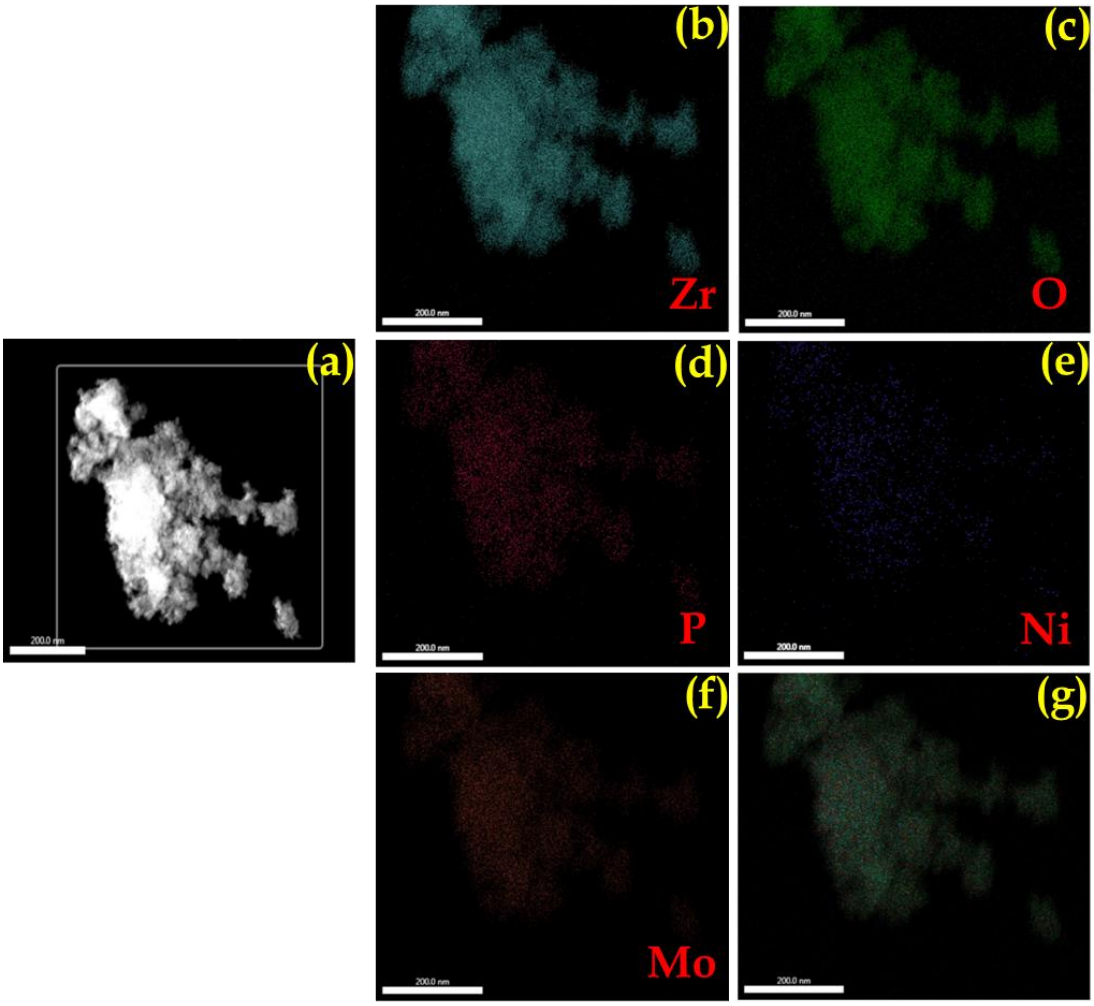

Figure 14. (a) HAADF-STEM of regenerated Ni- PMo_{12}/ZrO_2 and (b-g) elemental mapping of regenerated Ni-PMo_{12}/ZrO_2

XRD pattern of regenerated Ni–PMo_{12}/ZrO_2 and Ni–PMo_{12}/ZrO_2 are displayed in figure 15. The XRD spectra of R-Ni–PMo_{12}/ZrO_2 is undistinguishable with Ni–PMo_{12}/ZrO_2 which indicates retention of high dispersion of Ni. Absence of any characteristic peaks of Ni NPs may be due to very low amount of Ni (0.29 wt%) as well as high degree of dispersion beyond the detection limit of XRD.

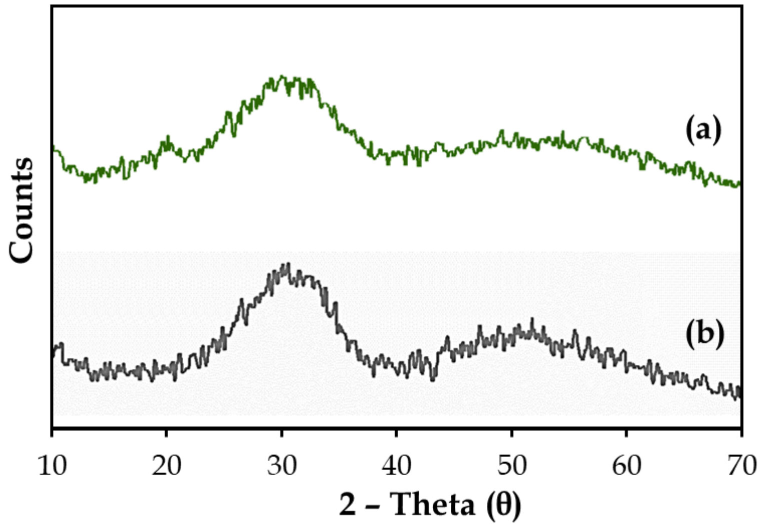

Figure 15. Powder XRD spectra of (a) fresh Ni-PMo_{12}/ZrO_2 (b) regenerated Ni-PMo_{12}/ZrO_2

The FT-IR spectra of regenerated and fresh catalyst are shown in figure 16. From the spectra, it can be seen that almost identical spectrum of the regenerated Ni–PMo_{12}/ZrO_2 was obtained without any significant shift in characteristic bands as compared to the fresh Ni–PMo_{12}/ZrO_2, indicating that the catalyst structure remains unaltered even after regeneration. However, the regenerated catalyst exhibit bands with slightly lower intensity as compared to the fresh one. This could be due to the substrates sticking to the catalyst, but it has no significant effect on the reutilization of the catalyst.

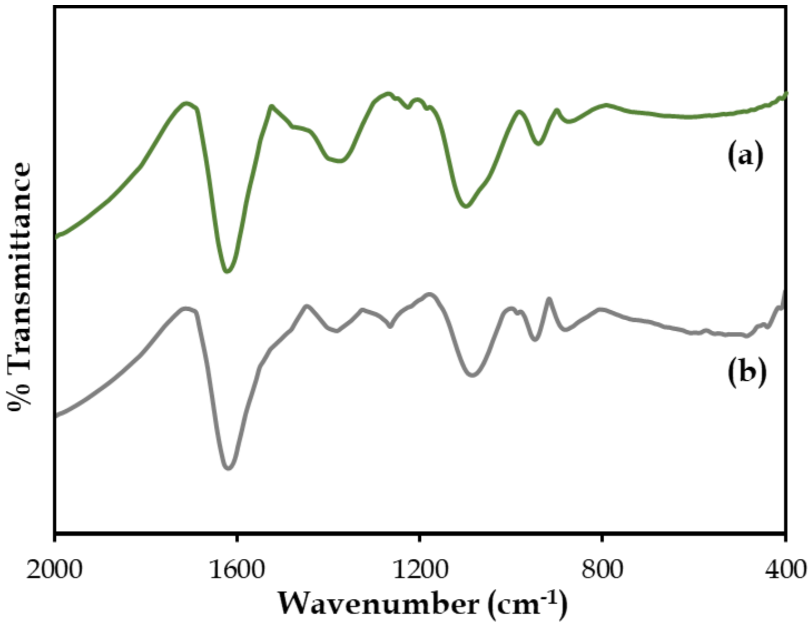

Figure 16. FT-IR spectra of (a) fresh Ni-PMo_{12}/ZrO_2 (b) regenerated Ni-PMo_{12}/ZrO_2

The EDX values of Ni (0.28 wt%) and Mo (wt%) for regenerated Ni–PMo_{12}/ZrO_2 are in good agreement with the fresh one (0.29 wt% Ni and 15.19 wt% Mo), which confirms that there was no leaching of Ni as well as Mo from the catalyst during the reaction. Also, elemental mapping shows (Figure 17) presence of all element.

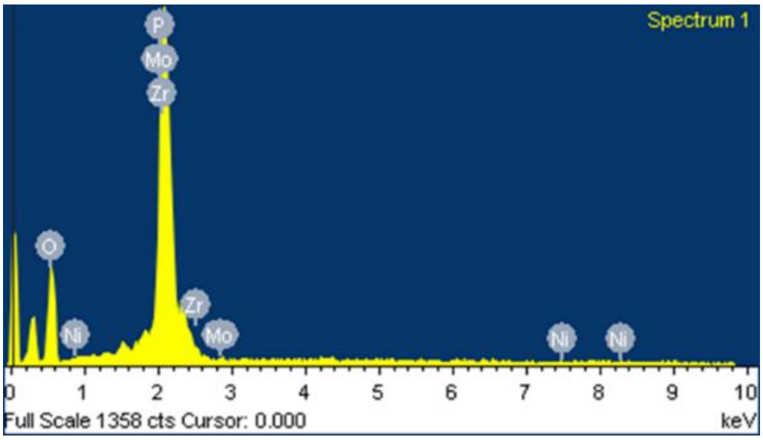

Figure 17. EDX mapping of regenerated Ni-PMo_{12}/ ZrO_2

Mechanistic investigation

To confirm formation of Ni(0), two sets of the reaction were carried out under optimized conditions. First, reaction was carried with Ni-PMo_{12}/ZrO_2 and FA (out without LA) and the obtained catalyst was found to be black in color instead of light green, similarly as shown in figure 9, which confirms that initially Ni(II) gets reduced to Ni(0) via catalytic dehydrogenation of FA. To confirm this, further reaction was carried out without catalyst (reaction only with FA and LA) under optimized conditions and after completion of reaction organic phase was analyzed by the GC. The obtained result show 0% conversion of LA, because at high temperature, FA dehydrogenates to form H_2O and CO without the presence of any metal [33]. This study confirms that when FA is used as an internal hydrogen source, metal is essential for H_2 generation and also it confirms that Ni(II) first reduce to Ni(0).

The plausible mechanism based on the above study is illustrated in Scheme 3. At the beginning of reaction initially, FA was dehydrogenated by adsorption on active catalytic surface (Ni) to form H_2 and CO which reduces Ni(II) to Ni(o) states. After that, the generated Ni(0) further form Ni-H_2 hydride species in the same way. Afterwards, LA is adsorbed on the Ni-H_2 site via oxygen of carbonyl group (C=O) and hydride transfer takes place to form 4-hydroxypentanoic acid as an intermediate product. Subsequently, the newly formed hydroxyl group and preexisting carboxyl group in 4-hydroxypentanoic acid would be react intramolecularly with each other to rapidly produce GVL and one molecule of H_2O through the self-condensation (dehydration) reaction. After that, the product is desorbed from the surface of the catalyst and the active sites will be free again to start another cycle.

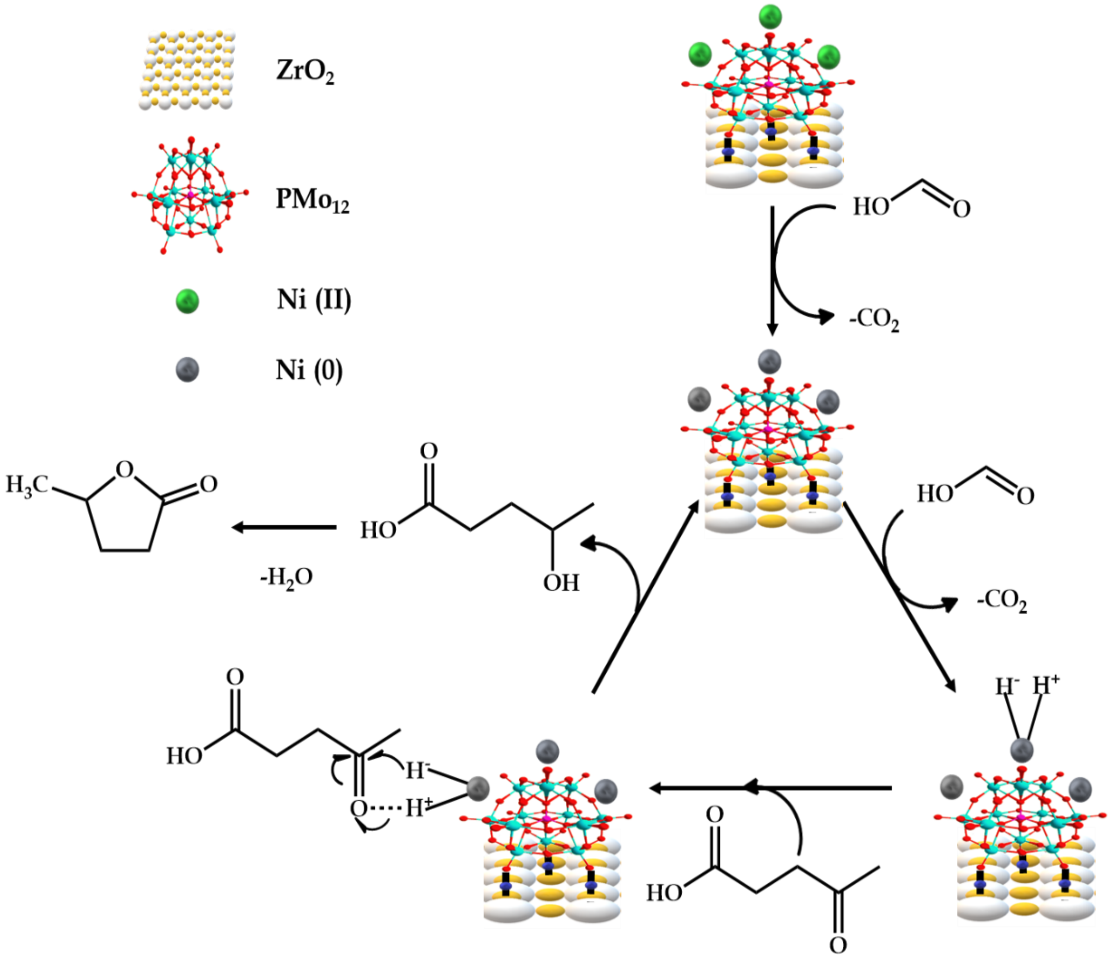

Scheme 3. Plausible reaction mechanism for LA hydrogenation

Comparison with reported system

The efficiency of the catalyst with reported system is also enumerated in Table 4 with respect to LA hydrogenation in terms of % conversion, reaction condition (such as H sources, solvent time and temp.). Form the table it can be seen that LA hydrogenation with different Ni nanoparticles (entry 1-7) required harsh reaction condition such as high catalyst amount, solvent, time and temperature. Also, they required high pressure of H_2 gas as hydrogen donor which difficult to operates. However, when reaction carried out with 2-propenol as internal H source as well as solvent which required high reaction time and solvent in terms achieve 70% GVL. In this direction present catalyst shows superior catalytic activity in terms of catalyst amount, H source, time and temp under solvent free condition as compared to amongst reported all catalyst.

Table 4. Comparison of styrene hydrogenation with reported systems

Sr. No.	Catalyst	Catalyst (mg)	LA (mmol)	H- source (mL/ bar)	Solvent	Time (h)	Temp. (°C)	% conversion
1	Ni/NiO[42]	0.2000	10	H_2 (20 bar)	Dioxane (100mL)	5	120	99
2	Ni/$Mg_2Al_2O_5$[43]	1.000	8.6	H_2 (30 bar)	Dioxane (40 mL)	1	160	99
3	Ni/Al-LDH[18]	0.1610	8.6	H_2 (30 bar)	Water (40 mL)	6	200	100
4	Ni/HZSM-5[27]	0.1000	4	H_2 (30 bar)	Dioxane (10 mL)	10	220	93
5	Ni/C-500[11]	0.0100	4.3	H_2 (10 bar)	Dioxane (20 mL)	5	200	98
6	Ni/Al_2O_3-CN-600[13]	0.0040	1	H_2 (5 bar)	THF (10 mL)	1	130	99
7	Ni@NCMs-700[23]	0.0025	1	H_2 (30 bar)	Dioxane (3 mL)	4	200	99
8	Ni/SiO_2-Al_2O_3[44]	0.0050	8.6	2-propenol (40 mL)	2-propenol (40 mL)	10	200	70
9	**Ni-PMo_{12}/ZrO_2**	**0.0050**	**5**	**FA (4.78 mL)**	**-**	**6**	**200**	**94**

CONCLUSION

- **Ni-PMo_{12}/ZrO_2** was successfully designed and evaluated for **aqueous phase solvent free hydrogenation of LA** using **FA** as an **internal** hydrogen source.
- High conversion **(94 %)** of LA using very less active amount of **Ni ($2.47*10^{-3}$ mmol)** with **TON of 1902** at 200 °C in 6 h was obtained.
- The in situ generation of **Ni(0)** was confirmed by **XPS** and **Ni(0)** active sites was exposed by **HRTEM, HAADF-STEM** analysis.
- The catalyst was reused up to **three cycles** without any **degradation or leaching.**

REFERENCES

[1] N. M. Maksimov, N. N. Tomina, P. S. Solmanov, A. A. Pimerzin, Pet. Chem., 58, 1045, (2018).

[2] F. Gao, S. Ni, Z. Niu, X. Tang, H. Yi, C. Wang, J. Environ. Chem. Eng., 9, 106190, (2021).

[3] D. Yu, W. Gao, S. Xing, L. Lian, H. Zhang, X. Wang, D. lou, RSC Adv., 9, 4884, (2019).

[4] J. Xu, X. Cao, J. Xia, S. Gong, Z. Wang, L. Lu, Analytica Chimica Acta, 934, 44, (2016).

[5] J. Jiang, R. Zheng, Y. Jia, L. Guo, M. Huang, J. Hu, Y. Xia, Anal. Chim. Acta, 493, 111044, (2020).

[6] R. Eisavi, F. Ahmadi, Sci. Rep., 12, 11939, (2022).

[7] B. P. Pinto, A. L. L. Fortuna, C. P. Cardoso, C. J. A. Mota, Catal. Lett., 147, 751, (2017).

[8] Z. Xue, Q. Liu, J. Wang, T. Mu, Green Chem., 20, 4391, (2018).

[9] L. T. Mika, E. Cséfalvay, Á. Németh, Chem. Rev., 118, 505, (2018).

[10] B. Mallesham, P. Sudarsanam, B. Venkata Shiva Reddy, B. Govinda Rao, B. M. Reddy, ACS Omega, 3, 16839, (2018).

[11] H. Xu, D. Hu, Z. Yi, Z. Wu, M. Zhang, K. Yan, ACS Appl. Energy Mater., 2, 6979, (2019).

[12] M. Al-Naji, M. Popova, Z. Chen, N. Wilde, R. Gläser, ACS Sustain. Chem. Eng., 8, 393, (2020).

[13] L. Jiang, G. Xu, Y. Fu, Green Chem., 23, 7065, (2021).

[14] R. Kuna, P. Balla, N. P. Rajan, B. Ponnala, S. Hussain, V. R. C. Komandur, React. Kinet. Mech. Catal., 135, 183, (2022).

[15] C. Ortiz-Cervantes, M. Flores-Alamo, J. J. García, ACS Catalysis, 5, 1424, (2015).

[16] M. Varkolu, V. Velpula, D. R. Burri, S. R. R. Kamaraju, New J. Chem., 40, 3261, (2016).

[17] A. M. Ruppert, M. Jędrzejczyk, O. Sneka-Płatek, N. Keller, A. S. Dumon, C. Michel, P. Sautet, J. Grams, Green Chem., 18, 2014, (2016).

[18] S. Gundekari, K. Srinivasan, Catal. Commun., 102, 40, (2017).

[19] X. Li, J. Li, X. Liu, Q. Tian, C. Hu, Catalysts, 8, 241, (2018).

[20] E. Soszka, H. M. Reijneveld, M. Jędrzejczyk, I. Rzeźnicka, J. Grams, A. M. Ruppert, ACS Sustain. Chem. Eng., 6, 14607, (2018).

[21] A. M. Ruppert, M. Jędrzejczyk, N. Potrzebowska, K. Kaźmierczak, M. Brzezińska, O. Sneka-Płatek, P. Sautet, N. Keller, C. Michel, J. Grams, Catal. Sci. Technol., 8, 4318, (2018).

[22] K. Sakakibara, K. Endo, T. Osawa, Catal. Commun., 125, 52, (2019).

[23] D. Liu, L. Zhang, W. Han, M. Tang, L. Zhou, Y. Zhang, X. Li, Z. Qin, H. Yang, Chem. Eng. J., 369, 386, (2019).

[24] A. García, R. Sanchis, F. J. Llopis, I. Vázquez, M. P. Pico, M. L. López, I. Álvarez-Serrano, B. Solsona, Energies, 13, 3448, (2020).

[25] B. Zada, R. Zhu, B. Wang, J. Liu, J. Deng, Y. Fu, Green Chem., 22, 3427, (2020).

[26] E. Soszka, M. Jędrzejczyk, I. Kocemba, N. Keller, A. M. Ruppert, Catalysts, 10, 1026, (2020).

[27] Z. Yi, D. Hu, H. Xu, Z. Wu, M. Zhang, K. Yan, Fuel, 259, 116208, (2020).

[28] L. Luo, X. Han, Q. Zeng, Catalysts, 10, 1096, (2020).

[29] Z.-X. Li, X.-Y. Wei, G.-H. Liu, X.-L. Meng, Z. Yang, S. Niu, D. Zhang, H.-S. Gao, Z.-H. Ma, Z.-M. Zong, Mol. Catal., 480, 110651, (2020).

[30] A. S. Amarasekara, Y. Maroney Lawrence, A. D. Fernandez, T. L. Grady, B. Wiredu, Biofuels, 12, 423, (2021).

[31] T. Jurado-Vázquez, A. Arévalo, J. J. García, Eur. J. Inorg. Chem., 2021, 445, (2021).

[32] L. F. Sosa, V. T. da Silva, P. M. de Souza, Catal. Today, 381, 86, (2021).

[33] R. Nie, Y. Tao, Y. Nie, T. Lu, J. Wang, Y. Zhang, X. Lu, C. C. Xu, ACS Catal., 11, 1071, (2021).

[34] A. Serrà, R. Artal, L. Philippe, E. Gómez, Langmuir, 37, 4666, (2021).

[35] H. Xu, D. Hu, M. Zhang, Y. Wang, Z. Zhao, Z. Jiang, H. F. Garces, K. Yan, ACS Appl. Nano Mater., 4, 3989, (2021).

[36] C.-C. Li, C.-H. Hsieh, Y.-C. Lin, Mol. Catal., 523, 111720, (2022).

[37] B. Zhang, H. Asakura, J. Zhang, J. Zhang, S. De, N. Yan, Angew. Chem. Int. Ed., 55, 8319, (2016).

[38] A. Patel, A. Patel, Catal. Lett., 152, 895, (2022).

[39] N. Bhatt, A. Patel, J. Mol. Catal. A: Chem., 238, 223, (2005).

[40] P. Sharma, A. Patel, Appl. Surf. Sci., 255, 7635, (2009).

[41] Chapter 8: Complexes on Oxide Supports in Oxidation Reactions, in: Y.I. Yermakov, B.N. Kuznetsov, V.A. Zakharov (Eds.) Studies in Surface Science and Catalysis, Elsevierpp. 283, (1981).

[42] S. Song, S. Yao, J. Cao, L. Di, G. Wu, N. Guan, L. Li, Appl. Catal. B: Environ., 217, 115, (2017).

[43] K. Jiang, D. Sheng, Z. Zhang, J. Fu, Z. Hou, X. Lu, Catal. Today, 274, 55, (2016).

[44] S. Gundekari, K. Srinivasan, Catal. Lett., 149, 215, (2019).